VILNIUS UNIVERSITY

CENTER FOR PHYSICAL SCIENCES AND TECHNOLOGY

TOMAS SEREVIČIUS

OPTIMIZATION OF MOLECULAR EMITTERS FOR NEW GENERATION OLEDS

SUMMARY OF DOCTORAL DISSERTATION

PHYSICAL SCIENCES, PHYSICS (02 P)

VILNIUS, 2015

The research has been carried out in 2011–2015 at the Institute of Applied Research, Vilnius University.

Scientific supervisor:

Prof. habil. dr. Saulius Juršėnas (Vilnius University, Physical Sciences, Physics – 02 P).

Doctoral thesis will be defended in the joint council of Vilnius University and Center for Physical Sciences and Technology.

Chairman: prof. Vincas Tamošiūnas (Vilnius University, Physical Sciences, Physics – 02 P).

Members:

Prof. habil dr. Nerija Žurauskienė (Center for Physical Sciences and Technology, Physics – 02 P).

Prof. habil. dr. Kęstutis Arlauskas (Vilnius University, Physical Sciences, Physics – 02 P).

Prof. dr. Martins Rutkis (University of Latvia, Physical Sciences, Physics – 02 P).

Prof. habil. dr. Sigitas Tamulevičius (Kaunas University of Technology, Physical Sciences, Physics – 02 P).

The official defence of the doctoral thesis will be held in the public session of the Defence Council of Physical sciences at 14 h on September 25, 2015, in 215 lecture room of Faculty of Physics, Vilnius University, Saulėtekio 9-III, LT-10222 Vilnius, Lithuania.

The summary of the doctoral thesis has been distributed on August 25, 2015.

The doctoral thesis is available at Vilnius University library and at the library of Center for Physical Sciences and Technology and also in the website of Vilnius University: *www.vu.lt/lt/naujienos/ivykiu-kalendorius*

VILNIAUS UNIVERSITETAS

FIZINIŲ IR TECHNOLOGIJOS MOKSLŲ CENTRAS

TOMAS SEREVIČIUS

MOLEKULINIŲ SPINDUOLIŲ OPTIMIZACIJA NAUJOS KARTOS ORGANINIAMS ŠVIESTUKAMS

Daktaro disertacijos santrauka

Fiziniai mokslai, fizika (02P)

Vilnius, 2015

Disertacija rengta 2011 – 2015 metais Vilniaus universitete, Taikomųjų mokslų institute.

Mokslinis vadovas – prof. habil. dr. Saulius Juršėnas (Vilniaus universitetas, fiziniai mokslai, fizika – 02P).

Disertacija ginama jungtinėje Vilniaus universiteto ir FTMC Fizikos mokslų krypties taryboje:

Pirmininkas: prof. Vincas Tamošiūnas (Vilnius universitetas, fiziniai mokslai, fizika, - 02 P).

Nariai:

Prof. habil dr. Nerija Žurauskienė (Fizinių ir technologinių mokslų centras, fiziniai mokslai, fizika, - 02 P),

Prof. habil. dr. Kęstutis Arlauskas (Vilnius universitetas, fiziniai mokslai, fizika, - 02 P),

Prof. dr. Martins Rutkis (Latvijos universitetas, fiziniai mokslai, fizika, - 02 P),

Prof. habil. dr. Sigitas Tamulevičius (Kauno technologijos universitetas, fiziniai mokslai, fizika – 02 P).

Disertacija bus ginama viešame Fizikos mokslų krypties tarybos posėdyje 2015 m. rugsėjo 25 dieną 14 valandą Vilniaus universiteto Fizikos fakulteto 215 auditorijoje, Saulėtekio al. 9, III rūmai, LT-10222 Vilnius, Lietuva.

Disertacijos santrauka išsiuntinėta 2015 m. rugpjūčio .25 d.

Disertaciją galima peržiūrėti Vilniaus universiteto ir Fizinių ir technologijos mokslų centro bibliotekose ir VU interneto svetainėje adresu: *www.vu.lt/lt/naujienos/ivykiu-kalendorius*

Santrauka

Organinė elektronika pastaruoju metu yra viena sparčiausiai besiplėtojančių puslaidininkių prietaisų krypčių dėl nuolat kuriamų naujų organinių junginių bei tobulėjančių prietaisų technologijų. Nežiūrint pasiekto didžiulio proveržio kuriant modernius molekulinius spinduolius bei OLED prietaisus, iki šiol tebevyksta įvairių tipų molekulinių puslaidininkių optimizavimas. Šiame darbe bus pristatoma dviejų spinduolių tipų, daugiafunkcinių fluorescencinių bei šiluma aktyvuotos uždelstosios fluorescencijos, įvairių darinių detali optinių, plevėdaros bei krūvio pernašos savybių analizė bei optimizavimas keičiant molekulinę struktūrą.

Pagrindinis šios disertacijos tikslas yra optimizuoti antraceno junginių struktūrą, siekiant suderinti visas perspektyviam OLED spinduoliui būdingas savybes: aukštą fluorescencijos kvantinis našumą, tinkamas plevėdaros savybes, susilpnintą fluorescencijos koncentracinį gesinimą bei aukštą krūvininkų dreifo judrį bei nustatyti, kaip šiluma aktyvuotos uždelstosios fluorescencijos spinduoliuose polinių fragmentų jungimo pokyčiai keičia tripletinių eksitonų apgrąžos efektyvumą.

Disertacija sudaryta iš penkių skyrių, suskirstytų į poskyrius. Pirmasis skyrius yra bendras įvadas, kuriame pateikiami darbo tikslai bei uždaviniai, darbo naujumas bei ginamieji teiginiai. Pirmame skyriuje taip pat pateikiamas disertanto su bendraautoriais publikuotų mokslinių straipsnių (įtrauktų, tiek ir neįtrauktų į disertaciją), pranešimų konferencijose pristatant disertacijoje pateiktus tyrimų rezultatus, sąrašas.

Antrame skyriuje pristatoma OLED spinduolių raida, pagrindiniai spinduoliu tipai ir jų pavyzdžiai, skirtingų spinduolių OLED efektyvumo pasiekimai.

Trečiajame skyriuje aprašomi bandinių paruošimo technologijos bei tyrimų metodai.

Ketvirtas skyrius susideda iš dviejų dalių. Pirmoje dalyje supažindinama su antraceno ir jo junginių optinėmis, krūvio pernašos ir taikymų OLED rezultatais, pateikiama literatūros apžvalga. Antroje dalyje, susidedančioje iš keturiu poskyriu, pristatomi eksperimentiniai rezultatai. Parodoma, kaip įvairios antraceno struktūros modifikacijos keičia optines, plevėdaros ir krūvio pernašos savybes, pateikiamos rekomendacijos antraceno struktūrai, leidžianti suderinanti tinkamas savybes OLED taikymams. Šio skyriaus rezultatai aprašyti [S1, S2 ir S3] darbuose.

Penktame skyriuje pateikiama karbazolo – triazino šiluma aktyvuotos uždelstosios fluorescencijos junginių ir iš jų padarytų OLED literatūros apžvalga, parodanti didelę junginių įvairovę bei eksperimentiniai rezultatai, parodantys, jog karbazolo-triazino junginiai, parinkus tinkamą polinių fragmentų jungtuką, yra efektyvus TADF spinduoliai. Šio skyriaus rezultatai aprašyti [S4] darbe.

Introduction

Currently, organic electronics is one of the most developing technologies of semiconductor devices. This direction is rapidly expanding due to the constant molecular engineering of novel organic compounds and advances in device technology. Currently, organic materials are used in organic light-emitting diodes (OLEDs), organic thin-film transistors, solar cells and sensors, due to its especial properties enabling low-cost manufacturing techniques such as wet casting or inkjet printing, allowing organic materials to use in large-area and flexible electronic devices. OLEDs are one of the fastest growing and well-developed applications of molecular semiconductors. According to *UBI Research*, the market size of only OLED compounds in 2020 will increase for 7 times as compared with 2015 and will reach 2.5 billion dollars [1]. One of the fastest growing applications of OLEDs is various screens, where the sales of solely widescreen TV's generated 280 million dollars in revenue and the market size increased for seven times in one year [2]. Another application of OLEDs, which is also rapidly emerging is indoor lighting. Recently, *Konica Minolta* announced very efficient OLED lamp with 131 lm/W power efficiency [3], which is comparable to those of inorganic light emitting devices. Similar modern lamps were installed in the library of Seoul National University, which is famous to be the first building in the world using only OLED-based lamps [4]. The constant decrease of OLED's prices will make them more and more usable in daily life.

Despite the great breakthrough in the creation of novel molecular emitters and OLEDs, still there are some weaknesses. One of the widely-used emitters is phosphorescent, of which the blue ones, due to the specific structure, suffers from the low stability and insufficient lifetime. One of the candidates to replace them are blue fluorescent emitters with remarkably higher stability and lifetime. These optimised fluorescent emitters possess perfect optical, thin-film forming and charge transport properties, what allows to use them in a highly efficient OLEDs, especially those utilising triplet-triplet annihilation, which efficiencies are comparable to phosphorescent OLEDs [5]. Few years ago, a new class of molecular emitters was offered, where the thermal activation of triplet excitons are used for the reversible intersystem crossing, leading to 100% of internal quantum efficiency [6]. Those extremely efficient TADF

emitters are successfully used in OLEDs, when its efficiency is the same as of phosphorescent ones however the lifetime is much higher. Despite this, the molecular structure of TADF emitters is quite complex and even small changes of molecular architecture leads to remarkable changes of optical properties.

In this work, the optimization of optical, thin-film forming and charge transport properties of two types of molecular emitters, fluorescent and TADF, will be presented.

Work goals and objectives. The optimization of fluorescent anthracene emitters is the first goal of this thesis. A great variety of anthracene compounds have been synthesized, however they have common drawbacks: either they possess high fluorescence quantum efficiency, but low charge carrier mobility, either high charge carrier mobility, but lower fluorescence efficiency and redshifted emission wavelength. We seek to modify the structure of anthracene with the help of non-symmetric substituents in such way, that the high fluorescence quantum efficiency, low fluorescence concentration quenching and high carrier mobility would be combined.

The second goal of this thesis is the optimization of nitrogen-based TADF emitters seeking to maximize the efficiency of delayed fluorescence. Recently it was found, that the efficient thermally activated reverse intersystem crossing in donor – acceptor systems is possible when the overlap of molecular orbitals in HOMO and LUMO is optimized. It allows to match low enough splitting of singlet ant triplet energy levels, which controls the reverse intersystem crossing, and high enough rate of the radiative recombination, which should be larger than that of non-radiative recombination. We present the evaluation of TADF efficiency in molecular systems and OLED devices.

Main objectives

1. To evaluate the impact of substitution of anthracene at 2-phenyl group and it's later stabilization with various heteroatoms to optical, thin-film forming and charge transport properties
2. To evaluate the impact of the non-symmetric substitution of anthracene at 9^{th} and 10^{th} positions with various aryl fragments to optical, thin-film forming and charge transport properties.

3. To estimate the impact of structural modifications of anthracene at 2^{nd}, 9^{th} and 10^{th} positions to radiative and non-radiative decay rates. To reveal the dominant non-radiative decay pathway, vibrational relaxation or intersystem crossing.
4. To optimize anthracene structure with suitable substituents at 2^{nd}, 9^{th} and 10^{th} positions.
5. To evaluate the efficiency of triplet thermal activation for polar carbazole – triazine compounds with different linker.
6. To test the performance of the most efficient compounds in OLEDs.

Novelty. All anthracene and carbazole-triazine compounds investigated in this work are new. Its optical, electroluminescence and photoelectrical properties are analysed for the first time. The recommendations for further optimization are also provided. Main new results are these:

1. 2-phenylanthracene derivatives cyclized with C, N, O and S atoms were systematically characterized. A possibility to tune the energy of HOMO in a broad range of 0.8 eV was showcased.
2. The dominating non-radiative recombination pathway was proved to be intersystem crossing, which rate remarkably increases after the conjugation extension at 2^{nd}, 9^{th} and 10^{th} positions of anthracene.
3. It was shown, that the additional modification of 9,10-arylanthracene at the second position with 2-phenyl group enhances thin film-forming properties and allows to obtain very high hole drift mobility.
4. The non-symmetric modification of 9,10-diphenylanthracene with small alkyl fragments at 9^{th} and 10^{th} positions together with non-conjugated substituent at the second position allows to suppress intersystem crossing, obtain amorphous thin films with very high hole drift mobility (up to 1×10^{-2} $(Vs)/cm^2$).
5. Linking carbazole and triazine polar fragments with carbazole instead of biphenyl makes triplet reverse intersystem crossing highly efficient.

Statements to defend:

1. Structural modifications of 9,10-diphenylanthracene core with 2-penthyl and *para*-methyl/hexyl substituents at the 9th and 10th positions allows to match high fluorescence quantum yield (up to 0.9), low fluorescence concentration quenching and very high hole drift mobility (1×10^{-2} (Vs)/cm^2).
2. The dominating pathway for the non-radiative recombination in 2,9,10-arylanthracene derivatives is intersystem crossing, which rate (also including that of vibrational relaxation) remarkably increases after the conjugation extension along the shorter and longer molecular axis due to the changes of higher triplet (T_n) energies.
3. Energy difference between S_1 and T_1 states in carbazole – triazine compounds decreases down to 90 meV when carbazole linker is used instead of biphenyl. Such compound is an efficient TADF emitter with delayed fluorescence efficiency of 0.25 and external quantum efficiency of 6% of light green OLED.

Layout of the thesis. The thesis consists of five chapters and reference list (152 titles). The text is written in Lithuania language on 144 pages with illustrations presented in 55 figures and 23 tables. An introduction, main goals and statements to defend as well as the articles and conference presentations concluding the presented data are listed at the **first chapter** of the thesis. The **second chapter** presents a short review of the application of molecular semiconductors as emitters in OLEDs, revealing the long-lasting research history, different types of emitters and basic principles. The experimental technique and sample preparation details are described in the **third chapter**. Original results are presented in **chapters 4** and **5**. The results of the optimization of anthracene compounds are showed in **Chapter 4**. TADF properties of carbazole-triazine derivatives, linked with different fragments, are disclosed in **chapter 5**. Both chapters include short overviews of the latest data about the properties and applications of anthracene derivatives and carbazole – triazine TADF compounds.

IV. MULTIFUNCTIONAL ANTHRACENES FOR OLED TECHNOLOGIES

Since the pioneering demonstration of electroluminescence in early sixties [5], a great work has been done in order to obtain truly efficient electroluminescence. It took almost 30 years until the breakthrough in organic electroluminescence inspired by Tang‘s and Van Slyke‘s [7] novel idea to use heterojunction of thin layers instead of bulk crystals. The later evolution of those modern OLEDs involved the further improvement of the device design and creation of new emitting materials. The first organic molecules used as emitters were simple fluorescent materials, capable to employ just 25% of created excitons. Later a new generation of phosphorescent emitters was suggested [8]. These Pt or Ir metal complexes had unique structure and photophysical properties with very efficient intersystem crossing resulting in up to 100% of excitons to be short-lived triplet states [9]–[12]. Novel OLEDs made of these phosphorescent emitters were extremely efficient with EQE reaching 20% and more [13], [14]. However, the complex molecular structure resulted in low stability, especially for the blue phosphorescent emitters [15]. The solution, which allowed to match 100% of internal quantum efficiency together with high stability, was proposed by Adachi *et.al.* in 2009 [16]. In this case, a novel class of efficient thermally activated delayed fluorescence materials was showcased. In TADF materials, the energy difference between S_1 and T_1 levels is low enough (usually lower than 100 meV) for triplet excitons to gain enough thermal energy to reverse them all into singlet ones. There are two types of TADF materials, donor-acceptor and metal (Cu, Sn) complexes [17], however donor – acceptor molecules [6], [18]–[20] are more desirable as they allow to get rid of complicated and less stable metal – organic complexes.

Despite the extremely high efficiency of electroluminescence from phosphorescent and TADF OLEDs, devices with simple fluorescent emitters (particularly the blue ones) are also highly desirable, since they are simple, stable, cheap and moderately efficient, especially those employing triplet – triplet annihilation [21]. Anthracene in one of the most studied blue emitter with high fluorescence efficiency, high stability and easy

modification [22], still very often used. A short overview of anthracene properties and the original results of the optimization of anthracene structure to in order to bear perfect optical, thin-film forming and charge transport properties will be presented in the next five subsections.

4.1. Various anthracene derivatives, its optical, thin-film forming, charge transport properties and applications in OLEDs

Anthracene is a planar and rigid molecule composed of three benzene rings. Electron density distribution is extended over the whole symmetric molecule [23], [24]. Due to the small π-conjugated electron system, anthracene absorbs and emits at 375 nm with a very low Stokes shift [25]. Its fluorescence quantum efficiency in solutions is about 0.3 [24] due to the high rate of intersystem crossing [26]–[29], which high rate is mediated by the unique arrangement of triplet states. The structural modifications at 9^{th} and 10^{th} positions (see fig 4.1) rearranges triplet energies and enhances the oscillator strength, enhancing fluorescence quantum yield up to the unity, like in case of 9,10-diphenylanthracene (DPA) [24]. However, anthracene core modifications with phenyl-side groups are insufficient to reduce intermolecular interactions and prevent crystallization [30]. The further modification of 9,10-phenyls with, e.g., *m*-terphenyl fragments [31] remarkably reduces crystallization and allows to obtain amorphous thin films. Remarkable enhancement of Φ_F of neat films and the increase of glass transition temperature was also achieved by the help of structural modifications at the second position by the introduction of highly twisted mesitilene fragment [32]. Similar results, like high Φ_F and good thin-film forming properties, are achieved also for bianthracene derivatives [5].

Anthracene compounds also show good charge transport characteristics. Those compounds modified at 9^{th} and 10^{th} positions with small aryls like naphthalene usually shows low hole drift mobility around $2\text{-}4\times10^{-7}$ $cm^2/(Vs)$ [33]–[36] probably due to partial crystallization, however the introduction more bulky aryls increases μ_h up to 3.1×10^{-4} $cm^2/(Vs)$ [37]. The most efficient hole transport is observed for anthracene derivatives modified with various nitrogen containing fragments. In this case, hole drift

mobility reaches up to 1×10^{-2} $cm^2/(Vs)$ [38], [39], however these nitrogen-based substituents tends to increase conjugation and redshift fluorescence up to 500 nm.

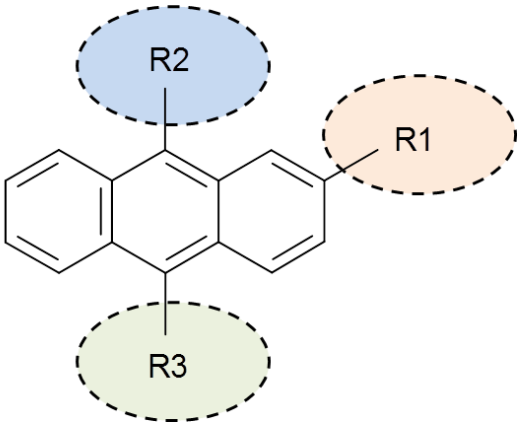

Fig. 4.1. Anthracene positions, where structural modifications were applied: 2nd (R1), 9th (R2) and 10th (R3).

Blue and efficient fluorescence, efficient charge transport and unique structure of triplet levels make anthracene very attractive emitter in OLEDs, utilizing triplet-triplet annihilation. Since the EQE of simple blue fluorescent OLEDs made from anthracenes reaches 5% [40]–[42], those OLEDs employing TTA boosts its efficiency up to almost maximum values of 12% [5].

As we have already showed, desirable blue anthracene derivatives composes perfect optical and charge transport properties, what makes then still attractive for the OLED applications. The next four subsections will provide original research results of optical, photoelectric and thin-film forming properties of various anthracene compounds modified at 2nd, 9th and 10th positions (see fig 4.1). The task was to optimize the molecular structure of anthracene derivatives to have high Φ_F, μ_h and low fluorescence concentration quenching.

4.2. Anthracene compounds modified at 2,9 and 10th positions

4.2.1. Properties of anthracene compounds modified at the second position

The alteration of anthracene structure at the second and the sixth positions is an effective way to reduce the intermolecular interactions [34], [41], thus a series of

anthracene derivatives introduced with 2-phenyl moiety and later cyclized with C, O, S and N atoms (see fig. 4.2) was synthesized by dr. P. Adomėnas group and thoroughly characterized [S1].

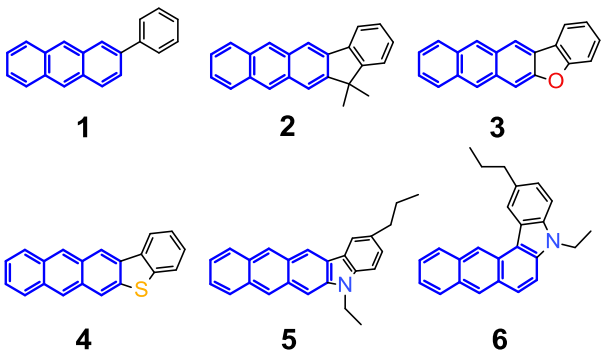

Fig. 4.2 2-phenylanthracene derivatives.

DFT modeling. The optimization of molecular structure revealed, that the anthracene compounds **2-6** are of flat geometry, while the 2-phenyl group in compound **1** is twisted for about 45°. The spatial electron density distribution is similar for all 2-phenylanthracene compounds. Conjugation is distributed over the whole molecule (see fig. 4.3) for all compounds **1-6** like in the unsubstituted anthracene [23]. The calculated $S_0 \rightarrow S_1$ oscillator strength was similar for all 2-phenylanthracene compounds (0.17-0.2), however the largest oscillator strength (0.27) was deduced for the compound **6**. Calculated $S_0 \rightarrow S_1$ transition energy gradually decreases from 3.40 eV in compound **1** to 3.18 eV in **5**. Correspondingly, calculated $S_0 \rightarrow T_1$ transition energy shifts from 1.24 eV in compound **1** to 1.17 eV in **5**. T_2 and higher-lying triplet states are situated in the proximity of S_1, thus can serve as the intermediate states promoting efficient deactivation of S_1 [26].

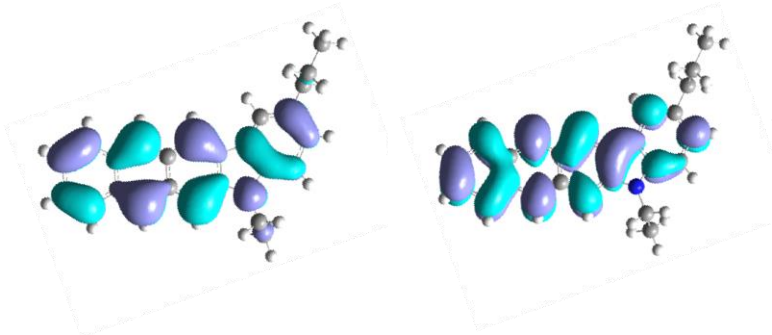

Fig. 4.3 Electron density distribution of compound **5** in HOMO and LUMO.

DSC analysis. Thin-film forming properties of 2-phenylanthracene derivatives were assessed by differential scanning calorimetry. Melting points (T_m) of 2-

phenylanthracene compounds **1**-**6** are in range of 132-326°C. The lowest T_m was for indolo-anthracene compounds **5** and **6**. The second heating scan revealed glass transition temperatures of 55°C, 34°C and 28°C for compounds **2**, **5** and. Almost all compounds, except **5**, showed crystallization peak at 90-304°C.

Optical properties. Absorption spectra of the derivatives contain multiple clearly resolved vibronic peaks separated by about 1400 cm^{-1} and are attributed to the rigid anthracene core (see fig. 4.4). Absorption peaks at 387 nm for compound **1** (with the redshift for 11 nm in respect of bare anthracene) and redshifts up to 479 nm for compound **6**, what is also supported by the DFT calculations. The molar absorption coefficients are in the range of 3560-9890 L $mol^{-1}cm^{-1}$. The results fairly well correlate with the absorptivity values of the biphenyl cyclized with the same bridging C, O, S and N atoms, resulting in fluorene, dibenzofuran, dibenzotiophene and carbazole compounds, respectively, showing the decisive role of heteroatom. As in the case of absorption spectra, fluorescence spectra of dilute solutions of the anthracene derivatives also demonstrated well-expressed vibronic structure and low Stokes shift due to rigid molecular core. Experimental data evidence that emission wavelength is gradually tuned from about 400 to 500 nm by cyclization of 2-phenylanthracene with carbon, oxygen, sulphur and nitrogen atoms, respectively. Fluorescence emission maxima of the neat films of the anthracene derivatives **1**-**6** are located in the range of 440-510 nm (fig. 5). Additional broad and structureless emission bands of excimer states peaked at 620-660 nm were observed in the spectra of compounds **4** and **6**. Fluorescence quantum yields of the anthracene compounds in the dilute solutions were found to range from 0.22 (for compound **4**) to 0.46 (for compound **6**) implying the dominance of non-radiative decay channel in the excited state relaxation processes. In case of neat films, Φ_F was comparable as in solutions (0.09-0.21) for compounds **1**-**3**, however it was remarkably lower for planar 2-phenylanthracenes **5**-**6**.

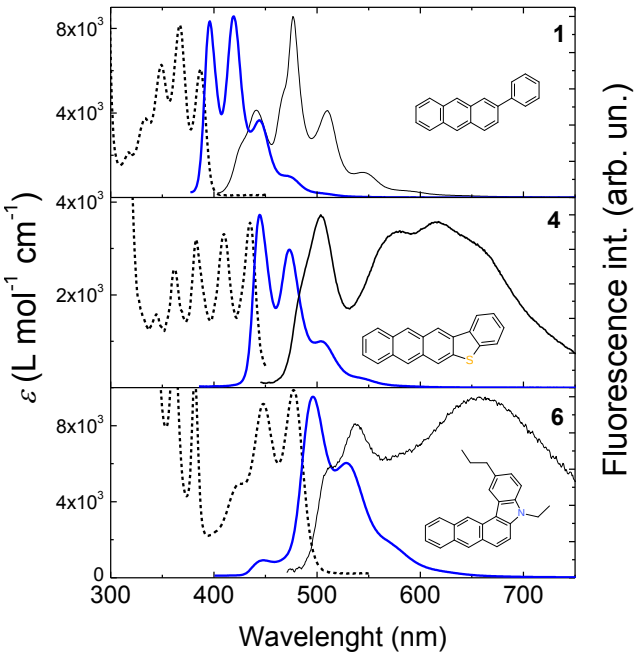

Fig. 4.4 pav. Absorption (dashed line) and fluorescence (solid blue line) spectra of the 2-phenylanthracene derivatives 1-6 in THF solutions and of the neat films (thin solid lines).

Excited state relaxation of **1**-**6** in dilute solutions was found to follow a single exponential decay profile with estimated decay time constant (τ_F) of 5.3-14.0 ns. Although similar τ_F as that for the unsubstituted anthracene was also detected for the compounds **1**, **2** and **3**, remarkably longer τ_F (8-14 ns) were estimated for compounds **4**, **5** and **6**. By analysing the changes in radiative and nonradiative decay time constants of unsubstituted anthracene the following trends were revealed: i) a slight decrease in radiative decay rate ($1/\tau_F$) with relatively unchanged nonradiative relaxation rate ($1/\tau_{nr}$) for the compounds **1**-**3**, ii) a strong decrease in radiative decay rate (more than a factor of 2) accompanied by a slight decrease in nonradiative decay rate for compound **4**, and iii) a strong decrease in nonradiative decay rate (more than a factor of 2.7) accompanied by a slight decrease in radiative decay rate for compounds **5** and **6**. A certain correspondence of these results to the Strickler-Berg rule [43], which predicts inverse proportionality of the extinction coefficient to the radiative decay time, can be envisaged. The cyclized compound 4 with a sulphur heteroatom features the longest τ_r (39.6 ns) while smallest ε, whereas the compound 2 with a bridging carbon atom exhibits the shortest τ_r (14.6 ns) and one of the largest ε. Variation in the nonradiative decay rate can be attributed to the changes in the intersystem crossing rate induced by the introduction of heteroatoms. Thus, cyclization with an N atom significantly reduces impact of the intersystem crossing.

Photoelectrical properties. Hole drift mobility measurements for the neat films of compounds **3**, **4** and **6** were impossible as they readily crystallized upon wet-casting, whereas the films of **1**, **2** and **5** demonstrated a pure amorphous phase. Values of μ_h were found to vary from 1.7×10^{-5} $cm^2/(Vs)$ (for compound **5**) to about 6.0×10^{-5} $cm^2/(Vs)$ (for

compounds **1** and **2**) at an electric field of 0.75 MV/cm (see fig. 4.5). These values of μ_h are comparable to other values obtained for anthracene derivatives [37].

Cyclization of 2-phenylanthracene with carbon, oxygen, sulphur and nitrogen atoms enabled tuning of the ionization potential (I_p) of the compounds in the broad range from 4.9 to 5.74 eV (see fig. 4.6). The highest I_p value was obtained for 2-phenylanthracene, meanwhile the lowest one was estimated for **6**. The ionization potential (or the HOMO energy if counted from the vacuum level) was found to decrease (increase) almost linearly with the absorption band edge of the anthracene derivatives, whereas LUMO energy remained nearly constant for all the derivatives. This is very important for the optimization of hole injection into the active layers, and thus for balancing electron and hole currents in the light-emitting devices.

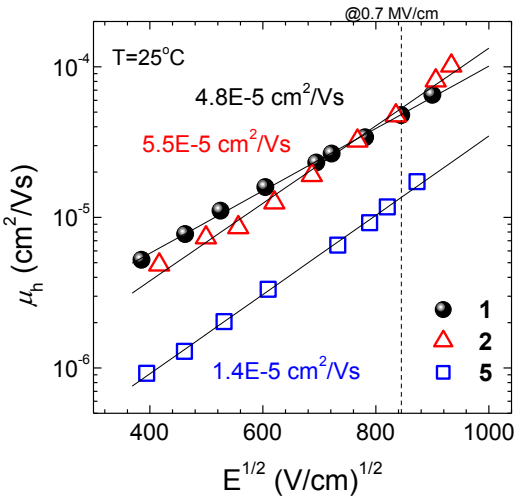

Fig. 4.5 Hole drift mobility dependence on the applied electric field for the neat films of compounds **1**, **2** and **5**. Lines are guides for the eye.

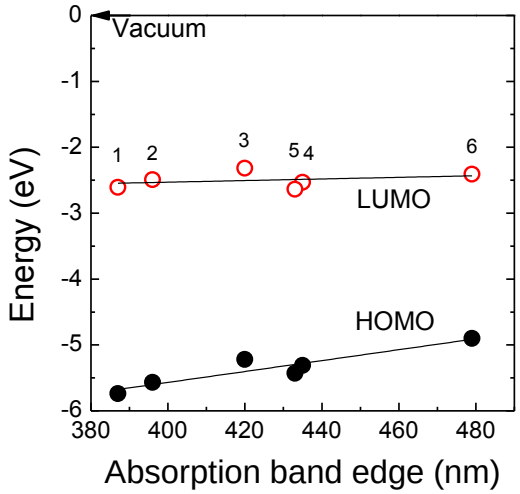

Fig. 4.6 HOMO (solid points) and LUMO (open points) energy levels of the anthracene derivatives **1**-**6**. Lines are linear fits of the experimental points.

In conclusion, the modification of anthracene core at the second position and later cyclization with various atoms does not allow to increase fluorescence efficiency, however it helps to reduce crystallization, obtain good hole drift mobility and enables to tune the energy of HOMO in a broad range of 0.85 eV.

4.2.2. Non-symmetric modification of anthracene compounds at 9th and 10th positions

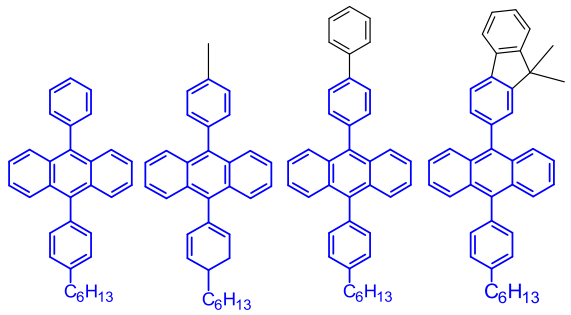

4.7 Anthracene compounds modified at 9th and 10th positions.

The next step was to try to non-symmetrically modify anthracene at the 9th and 10th positions to suppress crystallization and enhance fluorescence quantum yield. 10-(4-hexylphenyl) moiety was used the same for all compounds while the fragments in the 9th position were these: phenyl (**7**), *p*-tolyl (**8**), 9-(biphenyl-4-yl) (**9**) and 9-(9, 9-dimethyl-9*H*-fluorene-2-il) (**10**). Those compounds were synthesized by dr. P. Adomėnas group.

DFT modeling. The optimized molecular structure and electron density distribution of DPA derivatives **7** and **10** are shown in fig. 4.8. The twist angle of 9-substituent gradually decreases from almost 90° for DPA and compound **7** to 78.87° for compound **10**, while the fragment at the 10th position is less twisted. Electron density distribution in both HOMO and LUMO is almost the same as for the unsubstitued anthracene.

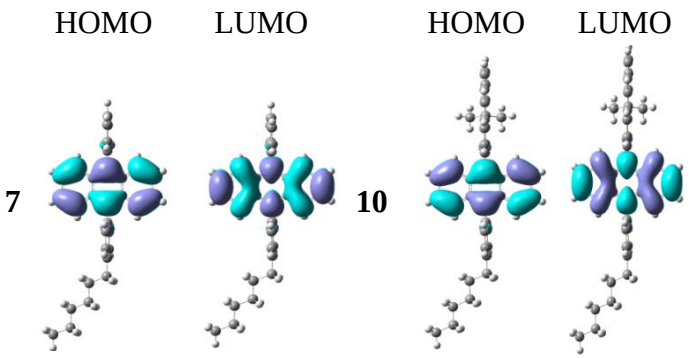

Fig. 4.8 Electron density distribution in HOMO and LUMO of DPA derivatives **7** and **10**. Calculated in B3LYP/6-311G (d,p) basis including THF ambient.

The calculated $S_0 \rightarrow S_1$ energy was gradually decreasing for compounds **7**→**10** due to increasing conjugation. The conjugation extension along the shorter anthracene axis was followed by the continuous increase of $S_0 \rightarrow S_1$ transition oscillator strength. The energy of T_1 state was of about 1.73 eV for all compounds, however the more prominent changes were observed for the energy of T_2. The second triplet level was situated ~100 meV above the S_1 for

compounds **7**-**9**, while T_2 emerged below the S_1 in compound **10** and is expected to act in intersystem crossing, lowering Φ_F.

DSC analysis. DPA derivatives **7**-**10** showed melting temperatures of 150-225°C and crystallization peaks at 100-155°C. Both temperatures were almost gradually increasing with the mass of fragment at the 9th position. Unfortunately, no glass transition was observed.

Optical properties. Absorption and fluorescence spectra of anthracene derivatives **7** and **10** are shown in fig. 4.9. The lowest energy vibronic bands in the absorption spectrum are observed at 394-396 nm with a very slight redshift after the introduction of biphenyl and fluorene substituents with extended conjugation. The molar absorption coefficient of the unmodified DPA is about 13400 almost the same as of its derivative **7**. The later modifications of DPA structure with more bulky biphenyl of diethyl-fluorene groups resulted in the increase of molar absorption coefficient up to 16000 due to higher oscillator strength and are in-line with the quantum chemical calculations. Fluorescence spectra peaked at 413-424 nm with slight redshift in respect of DPA (from 410 nm). The redshift of the fluorescence maxima are in line with the increase of the size of π-conjugated electron system and are also showed in the DFT calculations.

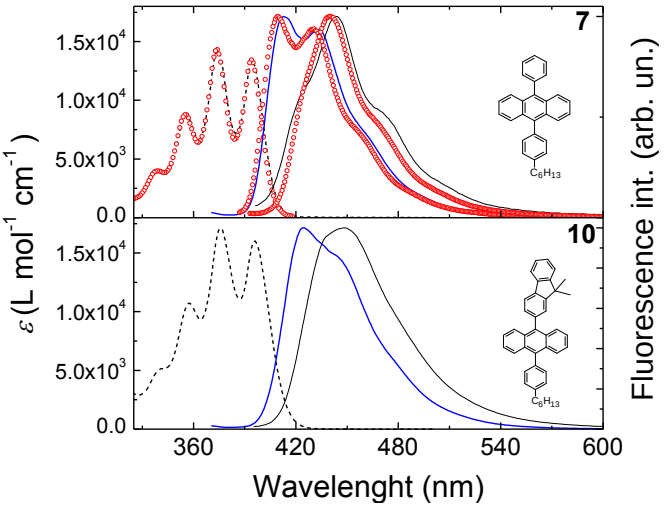

Fig. 4.9 Absorption (dashed line) and fluorescence (blue solid line) spectra of the anthracene derivatives **7** and **10** in dilute THF solutions and of the neat films (thin solid lines). The open dots represent absorption and fluorescence spectra of the unmodified DPA.

Fluorescence spectra of the neat films of the DPA derivatives **7**-**10** peaked at the deep blue region of the spectrum at 444-449 nm with 160-210 meV redshift in respect of the spectra in dilute solutions due to the presence of intermolecular interactions in the solid state. Fluorescence quantum yield of the dilute solutions of DPA derivatives **7**-**10** ranges from 0.58 to 0.78, remarkably higher, than of anthracene compounds **1**-**6**. An obvious decrease of Φ_F up to 0.15 - 0.27 was observed for the neat films. Drastically

decreased intermolecular distance in the solid states enables the intermolecular excitation migration and enhances the possibility of quenching at various defect-like sites, causing the decrease of Φ_F.

Fluorescence of dilute solutions of DPA derivatives **7-10** decays exponentially with time constants of 5.6-3.5 ns, up to two times faster than the unmodified DPA (6 ns). In case of neat films, a highly non-exponential behaviour with higher decay rate was observed, denoting the presence of energy transfer via exciton hopping through the localized states in disordered media. Despite the differences of the fractional decay times, all the derivatives showed very similar values of Φ_F.

Structural modifications of DPA by altering the substituents in the 9th and 10th positions resulted in changes of the rate of radiative and non-radiative processes (see Table 4.1) and the overall fluorescence decay rate.

Table 4.1 Fluorescence decay time constants (τ_F), quantum yields (Φ_F), radiative (τ_r) and nonradiative decay time constants (τ_{nr}) of the DPA derivatives **7-10** in 10^{-6} M THF solutions neat films and 0.1 wt% polystyrene films.

Com.	Dilute solution				Neat film		0.1 wt% in PS			
	τ_F (ns)	τ_r (ns)	τ_{nr} (ns)	Φ_F	τ_F(ns)	Φ_F	τ_F (ns)	τ_r (ns)	τ_{nr} (ns)	Φ_F
7	5.6	8.4	17.0	0.67	2.58 [77%] 4.75 [23%]	0.27	7.2	9.6	28.7	0.75
8	4	5.2	18.6	0.78	0.58 [48%] 1.9 [40%] 6.53 [12%]	0.15	5.2	7.5	16.8	0.69
9	4.2	5.8	15.2	0.72	0.91 [21%] 3.22 [75%] 14.22 [4%]	0.15	5.3	8.6	17.4	0.67
10	3.5	6.1	8.3	0.58	0.87 [52%] 2.55 [39%] 12.62 [9%]	0.2	4.8	7.8	12.2	0.61
DPA	6	6.4	100	0.94	0.64 [17%] 2.66 [44%] 7.62 [39%]	0.26	8.1	8.3	405	0.98

The modifications of DPA at both 9th and 10th positions resulted in the decrease of radiative recombination time (τ_r) up to 5.2 ns, 19% faster than in the unmodified DPA

(6.4 ns). The non-radiative recombination time in the unmodified DPA is very low (100 ns) due to the inefficient intersystem crossing and low rate of non-radiative recombination via torsional rotations. Unexpectedly, the rate of non-radiative recombination systematically increased up to 5.4-12 times for derivatives **7**-**10** causing the decrease of fluorescence quantum efficiency as compared to the un-substituted DPA. τ_{nr} was quite similar for compounds **7**-**9** (18.6-15.2 ns), thus it was remarkably lower (8.3 ns) for compound **10**, which had different triplet state picture, when T_2 was situated below S_1, making intersystem crossing very efficient. Almost no changes were observed for τ_r and τ_{nr} in dilute polymer films, where rotations of molecular fragments were restricted. This again shows that the intersystem crossing is the dominant mechanism of the non-radiative decay.

Photoelectrical properties. Since the neat films are in polycrystalline phase, its hole drift mobility is too low to measure due to very low charge transfer rate between polycrystalline sites. To solve this problem, DPA derivatives **7**-**10** were dispersed in polymer host by 50 wt % concentration when the undesirable crystallization was reduced. The highest hole drift mobility up to 4.1×10^{-5} $cm^2/(Vs)$ (at 1 MV/cm field) was measured for compound **9**, however compounds **7** and **10** demonstrated slightly lower μh up to 3×10^{-5} $cm^2/(Vs)$. The ionization potentials of the DPA derivatives **7**-**10** showed rather similar values of 5.72- 5.48 eV.

OLED device. High fluorescence efficiency and acceptable charge transport properties of DPA derivatives **7**-**10** makes them promising for OLED application. Dr. Arūnas Miasojedovas utilized several compounds in OLED structures (see fig. 4.10 a). OLED with compound **9** in the emissive (50% w.t.) and hole transport layer showed external quantum efficiency of 1.8%, almost twice more as it can be expected for OLED with fluorescent emitter. This enhancement of EQE was stimulated by the efficient triplet-triplet annihilation [21], evident from the electroluminescence transient (see fig. 4.19 b) bearing the long-lived delayed component.

a)

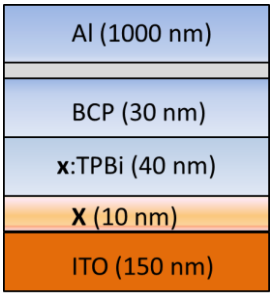

b)

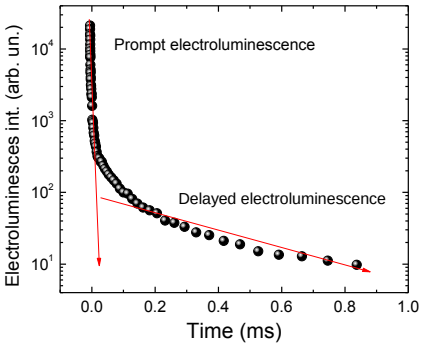

Fig. 4.10 a) OLED structure. x in this case is compound **9**. b) Electroluminescence decay transient of OLED device.

In conclusion, non-symmetric substitution of anthracene at 9th and 10th positions is a successful strategy for the enhancement of fluorescence quantum efficiency and those compounds are efficient emitters in OLED devices, however such modification is insufficient to reduce intermolecular interactions and obtain amorphous thin films.

1.2.3. Non-symmetric modification of anthracene compounds at 2, 9 and 10th position

The alteration of anthracene structure with 2-phenyl group enhanced thin-film forming properties and the non-symmetric modifications allowed to increase the fluorescence quantum yield, thus a series of 12 2,9,10-arylanthracenes, six compounds with 10-(2-naphtyl) group and six compounds with 10-biphenyl moiety, all of them having different fragments at the 9th position, was synthesized in dr. P. Adomėnas group and consistently characterized [S2].

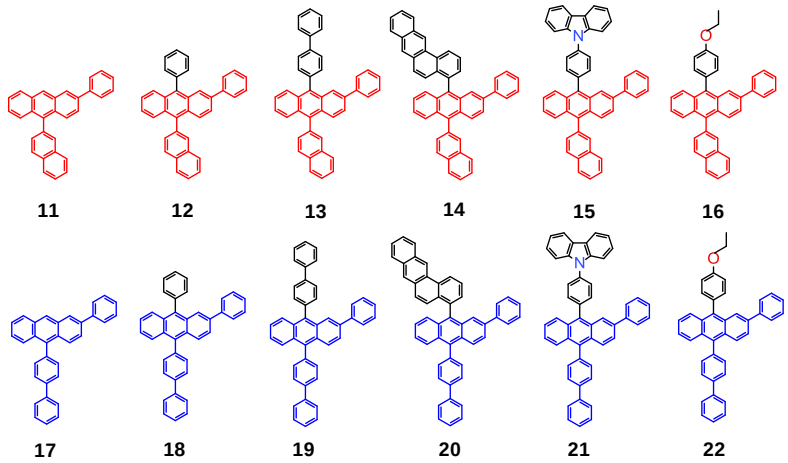

Fig. 4.11 List of synthesized non-symmetric 2,9,10-arylanthracenes featuring different type of 9,10-substituents.

DFT analysis reveals that 2-phenyl group is twisted at about 48° for all 2,9,10-arylanthracene compounds with the extended conjugation over the substituent. Aryl groups at 9^{th} and 10^{th} positions are twisted almost perpendicularly in respect of the anthracene core. This non-perpendicular geometry of substituents at the 9th and 10th positions results in the minor conjugation extension almost for all compounds, while the majority of the electron density is allocated over the anthracene backbone. The $S_0 \rightarrow S_1$ transition energy ranges from 3.01 eV for less conjugated compounds to 3.16 eV to for more conjugated counterparts. The energy of the first triplet state is in range of 1.7-1.77 eV for all 2,9,10-arylanthracene derivatives, similarly as it was observed for similar various anthracene compounds [44]. The T_2 state was observed at about 2.72 eV with minor changes of energy. The energy of the T_3 state was calculated to be below S1 in compounds **14** and **20** and almost equal for compound **11** while for the rest of compounds T_3 was situated above the S_1 state. The energy of T_4 state was higher than S_1 for all compounds except the mentioned **14** and **20** compounds where T_4 was situated below S_1. Those low-lying triplet states are expected to play crucial role during the excited state relaxation.

DSC analysis. Most of compounds showed similar thermograms when melting signals were observed in the first heating scan peaking at 146-330°C, similarly as in the second heating scan. A major part of anthracene compounds showed crystallization peaking at 59-260°C. Glass transition temperature of 30 and 60°C was obtained for compounds **17** and **22**, respectively. Although the rest of the compounds showed smooth wet casted films, due to the weak signal T_g could not be resolved.

Optical properties. The lowest energy vibronic bands in the absorption spectrum (see fig. 4.12) were observed at 387-406 nm with a slight redshift after the introduction of aryl substituents at the 9^{th} position. The variations of position of absorption band edge are in-line with the DFT calculations. The molar absorption coefficient of the 2,9,10-arylanthracene derivatives was in the range of 10500-15000 L $mol^{-1}cm^{-1}$, similar to the one of the unmodified DPA (ε=13400 L $mol^{-1}cm^{-1}$) and other similar anthracene derivatives presented earlier. Fluorescence spectra of dilute solutions peaked at 422-436 nm with lineshape similar to other anthracene derivatives like 2-phenylanthracene or DPA. No mirror image between absorption and emission spectra clearly indicates the existence of geometrical transformations of the molecular core upon the photoexcitation.

Emission spectra of neat films peaked at 442-461 nm with 0.08-0.24 eV redshift in respect of the emission in dilute solutions due to the presence of intermolecular interactions in the solid state. Fluorescence quantum yield of the dilute solutions of 2,9,10-arylanthracenes derivatives **11**-**22** ranges from 0.36 to 0.49, showing the domination of non-radiative recombination through molecular torsions via enhanced electron-vibron coupling or through intersystem crossing to the triplet states. Fluorescence quantum yield of neat films ranged in 0.03-0.13, down to the order of magnitude lower as compared to that of dilute solutions.

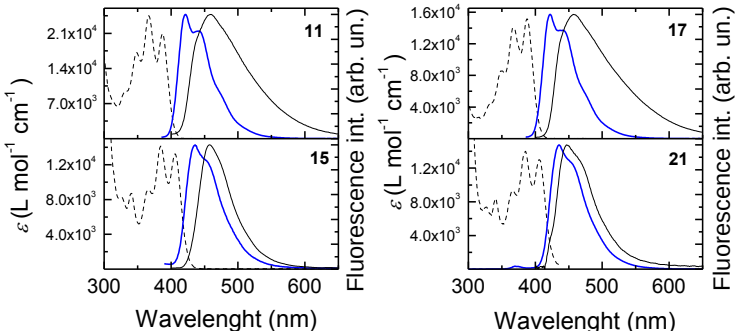

Fig. 4.12 Absorption (dashed line) and fluorescence (blue solid line) spectra of the 2,9,10-arylanthracene derivatives **11**-**22** in dilute 10^{-6} M THF solutions and neat films (thin solid lines).

Fluorescence decay transients exhibited very similar exponential decay in dilute solutions with time constants of 3.5-4 ns, remarkably faster than observed for various anthracene modifications (see chapters 4.2.1 and 4.2.2). Fluorescence decay transients of neat films of 2,9,10-arylanthracene derivatives shows non-exponential decay profile with very fast initial part due to efficient excitation migration via exciton hopping through the localized states in disordered media and non-radiative recombination at defect sites and slower later decay, which time constants are comparable to that of single molecule in dilute solution.

The minor variations of Φ_F are related to variation in the radiative rate constant and thus the oscillator strength of the lowest transition. The highest Φ_F of 0.46-0.49 was obtained for compounds with fastest τ_r (**13**, **14**, and **22**) and highest molar absorption coefficient. The non-radiative deactivation of excited state dominates for all 2,9,10-arylanthracene derivatives, resulting in Φ_F values below 0.5. Φ_F values were almost the same in a rigid matrix and in solution, indicating the minor role of vibronic relaxation and disclosing intersystem crossing as dominant non-radiative decay route, which rate is tuned by alignment of S_1 and T_n levels after the introduction of 2-phenyl group.

Photoelectrical properties. Hole drift mobility of 2,9,10-arylanthracene derivatives showed very high values exceeding 10^{-2} cm2/(Vs) at the field strength of about 1 MV/cm (see fig. 4.13). μ_h for compounds **11**, **13**, **14**, **18** and **20** is of 1×10^{-3} - 1×10^{-2} cm^2/(Vs) in the broad range of electric field strength (0.25-1.7 MV/cm). These values of μ_h are among the highest for the amorphous anthracene compounds. The continuous increase of μ_h with the applied electric field for all the 2,9,10-arylanthracene derivatives implies the governing role of energetic disorder. The values of ionization potential ranged ranging from 5.63 to 5.9 eV, slightly higher than of DPA derivatives **7-11**.

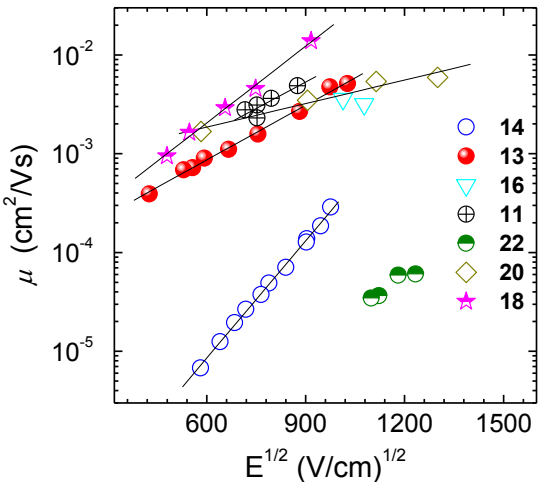

4.13 pav. Hole drift mobility as a function of the applied electric field in the neat films of the 2,9,10-arylanthracene compounds. Lines are guides for the eye.

In conclusion, the additional modification of 9,10-arylanthracenes with 2-phenyl group enhances thin-film forming properties and allows to obtain very high hole drift mobility up to 10^{-2} cm^2/(Vs), however such modification rearranges the triplet level scheme and enhances intersystem crossing rage, lowering fluorescence down to 0.5.

4.2.4. Optimization of DPA structure with small conjugated and non-conjugated substituents

Based on results presented in 4.2.1 – 4.2.3 chapters, showing that the modification of anthracene at the second position enhances thin-film forming properties, however conjugation extension along the shorter anthracene axis remarkably increases intersystem crossing rate and lowers Φ_F, two series of conjugated and non-conjugated substituents at the second position and small alkyl-aryl fragments at the 9th and 10th positions (see fig. 4.14). These compounds were synthesized in dr. P. Adomėnas group and consistently characterized [S3].

DFT analysis. Phenyl groups at the 9th and 10th positions in the studied nonsymmetrically substituted DPA compounds **23-28** forms 80° angles in respect of anthracene core, 2-phenyl group (**23-25)** is twisted in respect to the core by about 55°. Generally, the spatial distribution of electron density in the ground and excited states resemble that of the unsubstituted anthracene. Only a small fraction of molecular orbitals extends towards the substituents. The $S_0 \rightarrow S_1$ transition energy of compounds **23-25** was 3.115-3.124 eV and slightly decreases down to 3.069-3.091 eV for more conjugated compounds **26-28**. The oscillator strength of $S_0 \rightarrow S_1$ transition was up to 30% higher for less conjugated compounds **26-28.**

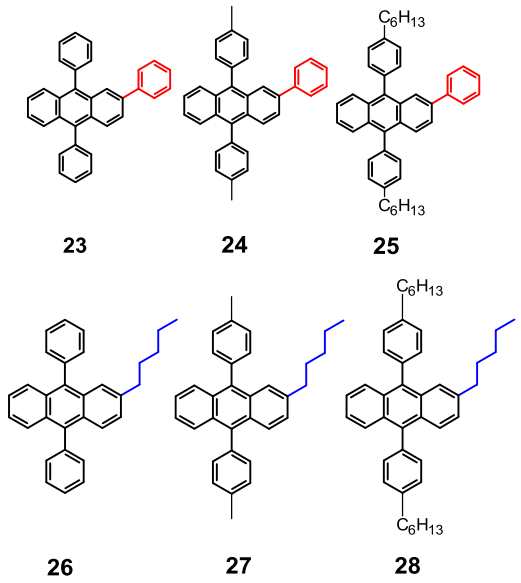

Fig. 4.14 Chemical structures of the DPA derivatives **23-28**.

A similar trend was observed also for triplet states. T_1 level has similar energy to other anthracenes at about 0.995/0.98 eV (the calculations were performed in vacuum, so the obtained energies are lower) and decreased for more conjugated compounds **26-28.** Similarly, the second triplet state also had lower energy for more conjugated compounds **26-28**, 1.96 eV as compared to 2.05 eV. Although the differences in singlet and triplet energies of the compounds **23-25** and **26-28** are not significant, they can notably affect the rate of intersystem crossing thereby severely impacting photophysical and photoelectrical properties of the compounds.

DSC analysis. All the DPA compounds **23-28** exhibited similar DSC thermograms by demonstrating melting signal only in the first heating scan with peaks centred at 193-209°C and 60-105°C for compounds **23-25** and **26-28**, respectively. An absence of crystallization peaks during the cooling indicated that the compounds were transformed into an amorphous phase. The second heating scan revealed glass transition temperatures of 7-92°C for compounds **23-25** and -24-(-1)°C for compounds **26-28**. The introduction of 2-penthyl substituent remarkably lowered the T_m and T_g.

Optical properties. The lowest energy vibronic bands in the absorption spectrum (see fig. 4.15) of the 2-phenyl substituted DPA compounds **23-25** peaks at 405 nm, whereas the bands of the 2-penthyl substituted counterparts **26-28** are shifted more in the UV (at about 391 nm) due to the worse π-conjugation of the substituent. The molar extinction coefficient of the derivatives does not exceed that of the unsubstituted DPA (ε = 13400 L·mol^{-1}·cm^{-1}) and varies between 10000 and 13000 L·mol^{-1}·cm^{-1}.

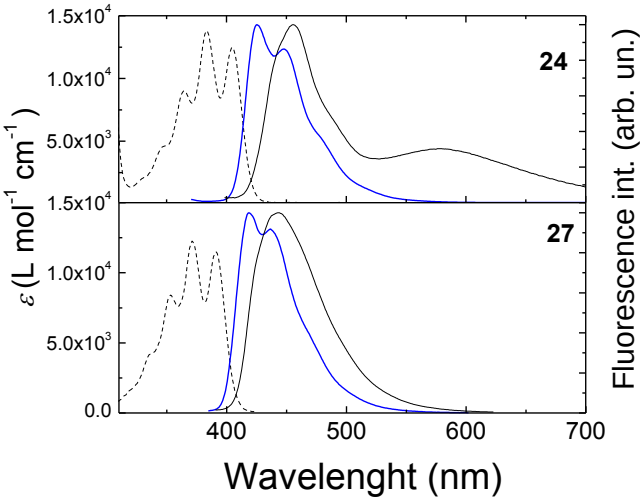

Fig. 4.15 Absorption (dashed line) and fluorescence (blue solid line) spectra of the DPA derivatives **23-28** in dilute 10-6 M THF solutions and neat films (thin solid lines).

In accordance with the absorption spectra, fluorescence bands of more conjugated 2-phenyl-substituted DPA derivatives **23-25** are located at 422-426 nm, and thus are slightly redshifted as compared to those of the less conjugated 2-penthyl-substituted DPA counterparts **26-28** peaking at 416-421 nm, still deep blue. The mirror image between absorption and emission implies flexibility of the molecules and geometrical transformations occurring in the excited state in agreement with DFT calculation results. Fluorescence spectra of the neat films of the DPA derivatives **23-28** are slightly redshifted as compared to the spectra of their dilute solutions, which is due to the enhanced intermolecular interactions in the solid state. The films of the compounds **23-26** and **26-28** emit in the deep blue with maxima positioned at 453-456 nm and 441-450 nm, respectively.

Estimated fluorescence quantum yields of the DPA derivatives in dilute solutions were found to range from 0.45-0.49 for compounds **23-25** to 0.68-0.71 for compounds **26-28**. Φ_F of the neat films of the DPA derivatives was found to be considerably lower as those of their dilute solutions. Φ_F values of only 0.03-0.06 were obtained in 2-phenyl-substituted DPA compounds **23-25**. Obviously, only 2-fold drop in Φ_F observed for the neat films of compounds 4-6 as compared to their solution in contrast to roughly 10-fold drop observed for the compound **23-25** neat films indicates that the 2-penthyl moieties more effectively suppress aggregate formation as the 2-phenyl groups.

Fluorescence transients of the DPA derivatives **23**-**28** in dilute solutions follow single-exponential decay profile with τ_F of 5.0-6.2 ns similar to that of the unsubstituted DPA (τ_F=6.0 ns). In contrast, fluorescence transients of the neat DPA films exhibit highly non-exponential decay profiles. The non-exponential temporal profile accompanied by the redshifted fluorescence bands of the solid films is a clear signature of energy transfer occurring via exciton hopping through the localized states in disordered or partly disordered media.

Despite the similar fluorescence lifetimes, the series of DPA derivatives **23**-**28** show different behaviour of the radiative and non-radiative relaxation processes. Radiative decay time of the compounds is rather similar, i.e. average is 10.8 ns and 8.5 ns for the compound series **23**-**25** and **26**-**28**, respectively, whereas non-radiative time constant of these series differ by a factor of 2. τ_{nr} was found to be significantly shorter, and so the non-radiative relaxation rates faster, for the 2-phenyl-substituted DPA compounds **23**-**25** (τ_{nr} = 9.7 ns) as compared to those bearing 2-penthyl moiety, compounds **26**-**28** (τ_{nr} = 18.9 ns). To prove the nature of non-radiative recombination, Φ_F, τ_r and τ_{nr} were estimated in rigid polymer matrix, where molecular rotations restricted. Φ_F of the compounds **23**-**25** with the 2-phenyl moieties in dilute solution and PS matrix showed slight increase in the rigid matrix (from ~0.47 in solution to ~0.60 in PS matrix) mainly due to the decreased non-radiative decay time. However a similar increase of Φ_F is also observed for **26**-**28** derivatives without these moieties (from ~0.69 in solution to ~0.84 in PS matrix), where torsional motions are absent. This result clearly rules out the intramolecular torsions as the key-mechanism responsible for enhanced nonradiative relaxation of the compounds **23**-**28** and suggests enhanced intersystem crossing to triplet states to play the decisive role.

Fluorescence concentration quenching. Fluorescence concentration quenching is a key factor, which determines the applicability of a compound for OLED application. Utilization of an emissive material at high concentrations (typically of more than a few percent) in a host material is limited by the enhanced molecule interaction, and in severe cases, physical molecule agglomeration activating exciton migration and migration-induced exciton quenching, and therefore is detrimental to the device performance. Concentration quenching in the DPA derivatives was evaluated by dispersing DPA

molecules in a rigid and transparent polystyrene (PS) host while measuring fluorescence quantum yield changes *(Vs)* concentration in the broad range of concentrations 0.1-100 wt % (see fig. 4.16). All the DPA derivatives **23-28** demonstrated negligible fluorescence concentration quenching up to 8 wt % in PS. The rate of concentration quenching for the compounds **23-25** featuring 2-phenyl substituent is very similar (Figure 8a). Φ_F quenches just lightly faster as compared to that of the unsubstituted DPA. The quenching rate of Φ_F for DPA compounds **26-28** with increasing concentration is slower as compared to that of the reference DPA, and moreover, slower than that of 2-phenyl substituted compounds **23-25.**

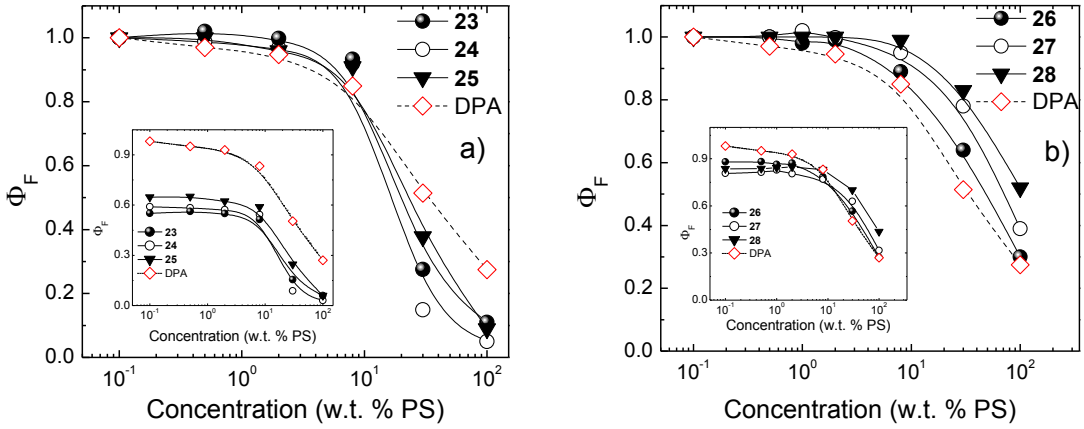

Fig. 4.16 Normalized fluorescence quantum yield of the DPA compounds **23-28** as a function of their concentration in PS matrix. Lines are guides to the eye. Absolute values of fluorescence quantum yields are displayed in insets.

Photoelectrical properties. Introduction of the additional phenyl or penthyl moieties at the 2nd position and the methyl groups at the para positions of 9,10-phenyls (compounds **23**, **24**, **26**, **27**) completely suppressed DPA crystallization and ensured formation of amorphous neat films. These nonsymmetrically modified DPA derivatives **23-28** expressed very high hole drift mobilities well exceeding 10×3 $cm^2/(Vs)$ at 1 MV/cm electric field. The obtained drift mobility values varied from 4.6×10^{-3} $cm^2/(Vs)$ in the compound **23** up to almost 1×10^{-2} $cm^2/(Vs)$ in the compound **26** at an electric field of 1 MV/cm. The estimated ionization potentials showed very similar values 5.74-5.9 eV comparable to those reported for 2-phenyl-substituted anthracenes (compounds **11-22**).

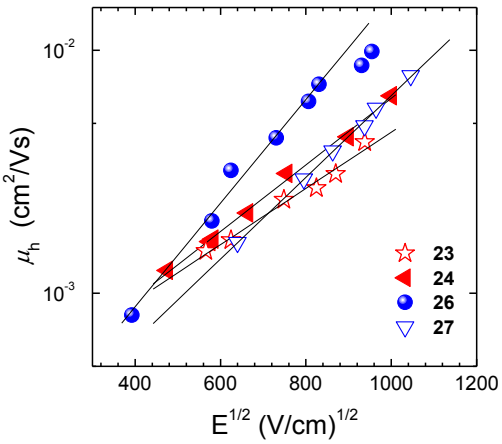

4.17 pav. Hole drift mobility as a function of the applied electric field in the neat films of the DPA compounds compounds **23**-**28** . Lines are guides for the eye. The average film thickness is indicated.

In conclusion, the consecutive optimization of anthracene structure revealed that introduction of non-conjugated substituent at the second positions and the modification of 9,10-phenyls with aliphatic chains allows to obtain high fluorescence quantum yield and low fluorescence concentration quenching. The dominating pathway for the non-radiative recombination was proven to be intersystem crossing. These highly efficient anthracenes also shows very high hole drift mobility, making those anthracene derivatives highly promising for OLEDs.

V. THERMALLY ACTIVATED DELAYED FLUORESCENCE EMITTERS FOR OLED APPLICATIONS

5.1. Nitrogen heterocyclic compounds for thermally activated delayed fluorescence

One of the ways to utilize triplet excitons and obtain highly efficient electroluminescence is to exploit thermal energy [16]. A particular class of materials, called thermally activated delayed fluorescence emitters, has low energy difference between S_1 and T_1 states, thus triplet excitons can undergo thermally activated reverse intersystem crossing back to singlets [45]. The low ΔE_{ST} is achieved in donor-acceptor materials or metal (e.g. Cu, Sn) complexes, however donor-acceptor molecules are more promising because of metal-free structure [17]. The key requirement for low ΔE_{ST} for those molecules is the separation of molecular orbitals in HOMO and LUMO, what is succesfully utilised in molecules with polar fragments [6].

There is a great variety of polar fragments are used in TADF molecules, like carbazole, triazine, acridine, tiophene, triphenylamine [17], which are separated by various non-polar fragments or by forming spiro structures. Due to the electron-deficient nature of aromatic systems containing an electronegative nitrogen atom, N-containing arenes with promising electron affinities, are especially promising as electron-accepting moieties in the molecular scaffold of high performance TADF materials. Blue TADF OLEDs based of carbazole-triazine compounds achieves external quantum efficiencies up to 19% [15] and shows enhanced stability as compared to phosphorescent devices.

In the next section original results of the optimization of carbazole-triazine structure to be the efficient TADF emitter will be presented. Two different linkers, carbazole and biphenyl, will be tested in order to show how slight changes of molecular structure affects TADF properties. The research of TADF emitters was performed in OPERA research centre, Kyushu University under the supervision of prof. Chihaya Adachi and in collaboration with dr. Tetsuya Nakagawa.

5.2. The effect of linking topology for TADF characteristics of carbazole – triazine compounds

We present the detailed study of photophysical characteristics including fluorescence solvatochromical effects and temperature dependent fluorescence to verify the TADF behaviour of **CzT** (see fig. 5.1) and its application as a TADF emitter for efficient OLEDs. To reveal the importance of molecular configuration for giving effective TADF, a model carbazole–triazine compound **PhCzTAZ** possessing highly twisted structure of carbazole and triazine fragments was analysed for comparison. The details of synthesis and characterization are described in [S4].

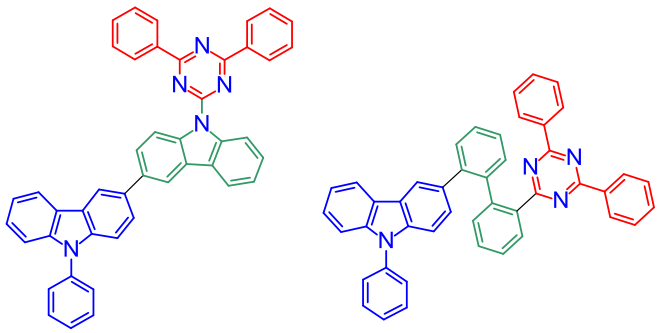

Fig. 5.1 Molecular structures of **CzT** and **PhCzTAZ**.

DFT analysis. To understand the electronic structure of **CzT** and **PhCzTAZ**, density function theory (DFT) calculations were performed at a B3LYP/6-31G(d) level for the geometry optimization. HOMO orbital of both **CzT** and **PhCzTAZ** is mainly populated over the dicarbazole and peripheral phenyl moiety, while the LUMO orbital is mainly localized on electron-deficient phenyl-triazine fragment, however the molecular structure of **PhCzTAZ** structure is much more distorted (see fig. 5.2). These result reveals that both **CzT** and **PhCzTAZ** has evident spatial separation of HOMO and LUMO and low ΔE_{ST} of 68 and 96 meV, respectively, which is beneficial for efficient TADF.

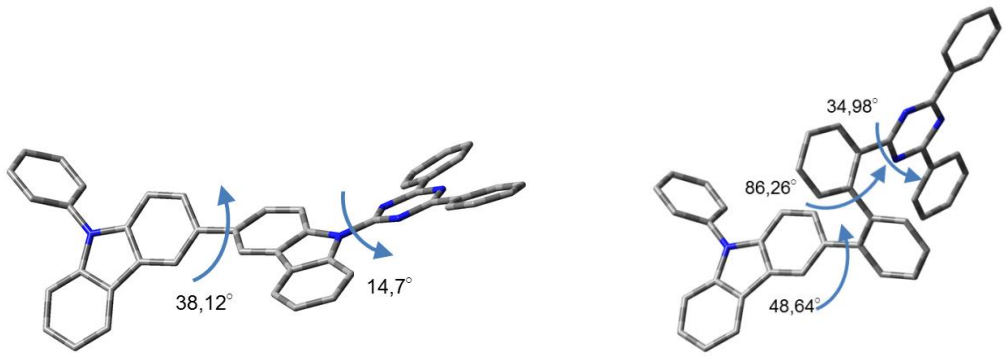

Fig. 5.2 The optimized Molecular structures of **CzT** and **PhCzTAZ**.

Optical properties. Photoluminescence spectra of 1.5×10^{-5} M **CzT** solution in toluene and hexane are shown in fig. 5.3. The PL spectrum of **CzT** in hexane exhibits a vibronic structure with emission peaks at 453 and 472 nm. There is an obvious change of spectral features of CzT in polar, in which the full width at half maximum (FWHM) increased from 86 to 105 nm and the spectrum became structureless with the emission maximum centred at 512 nm. Clearly, fluorescence emission of **CzT** showed dependence on the polarity of solvent. The fluorescence spectra of **PhCzTAZ** with the vibronic structure were observed in hexane and toluene with peaks at 445/468 nm and 453/469 nm, respectively. The existence of a vibronic structure in the emission spectrum with a limited red-shift as the solvent polarity increases implies that the emission of **PhCzTAZ** originates from the LE states, and not the ICT states.

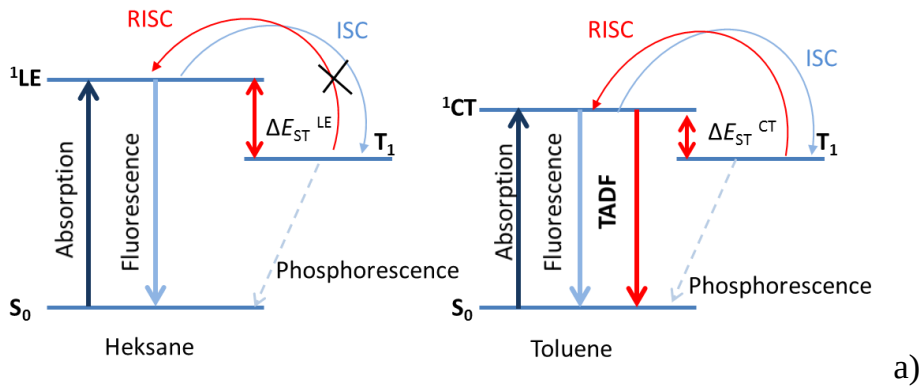

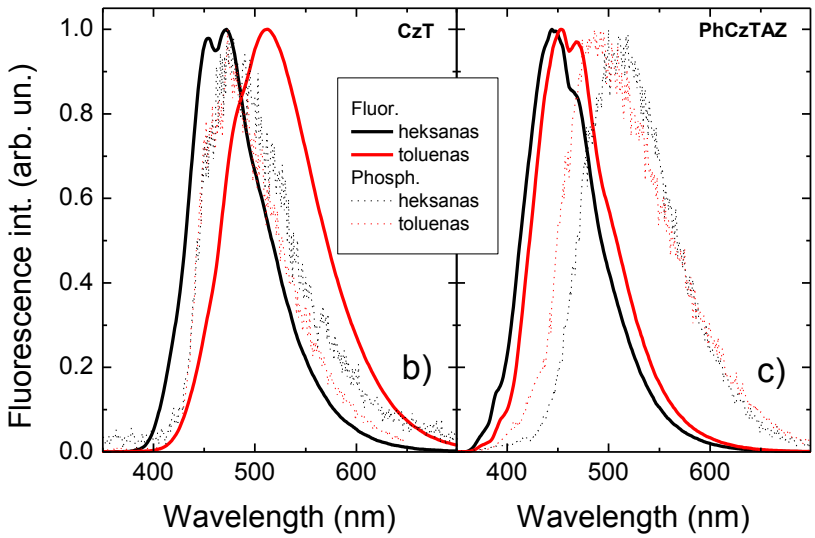

Fig. 5.3 (a) Energy levels diagram and observed transitions of **CzT** in hexane and toluene. b) Room temperature fluorescence (solid lines) and phosphorescence (dotted lines) spectra in hexane (black line) and toluene (red line) of **CzT** (b) and **PhCzTAZ** (c)**.**

The phosphorescence peak position of **CzT** cantered at 475 nm is almost independent of the solvent polarity. Similar solvent-independent behaviour of phosphorescence spectra of **PhCzTAZ** was observed. The energy difference between the singlet S_1 and triplet T_1 energy levels calculated from the onsets of the fluorescence and phosphorescence spectra of **CzT** was estimated to be 85 meV in hexane and only about 8 meV in toluene. In hexane, the lowest excited state of **CzT** is assigned to the LE state. Therefore, the energy difference between the LE state and T_1 state is large, which will impede the up-conversion process at room temperature. On the other hand, the lowest excited singlet state of **CzT** is switched to the CT state due to the stabilization in polar toluene. The resulting lower ΔE_{ST} in toluene enables the up-conversion of triplet excitons to the singlet CT state at room temperature (see fig. 5.3 a).

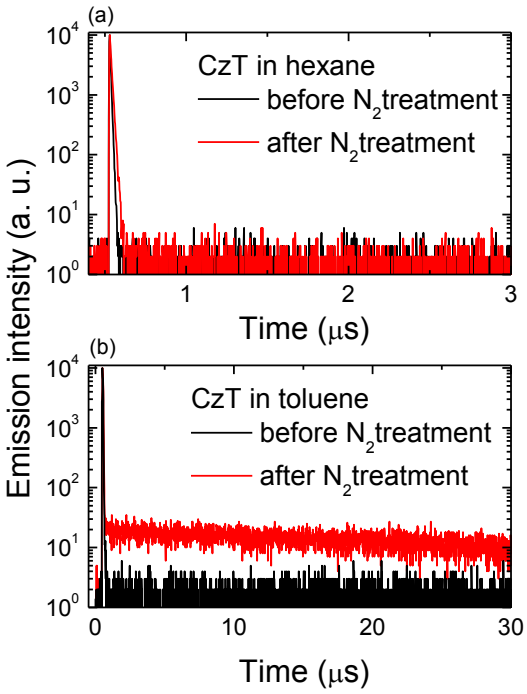

Fig. 5.4 Fluorescence decay transients of **CzT** in hexane solution(a) and in toluene solution(b). Black line and red line show the profiles before and after the nitrogen bubbling, respectively.

The model carbazole–triazine compound **PhCzTAZ** also exhibited solvent polarity independent phosphorescence and rather limited CT behaviour. The lowest excited singlet state of **PhCzTAZ** is believed to be localized at the LE state. Therefore, relatively high values of ΔE_{ST} (480 meV in hexane and 200 meV in toluene) were observed for **PhCzTAZ**, thus such high values make the up-conversion of triplet excitons impossible.

Fig. 5.4 depict the fluorescence decay transients of **CzT** before and after N_2 treatment. N_2 treatment can eliminate the possibility of deactivation of photoexcited **CzT** via quenching by low-energy triplet states of oxygen. Single exponential decay with no delayed fluorescence was observed from oxygen-containing and N_2-treated transients of **CzT** in hexane. On the other hand, an intense delayed fluorescence emission of CzT in toluene with a decay time of 42.6 μs emerged after N_2 treatment. Oxygen-sensitive behaviour was also observed for the fluorescence quantum yield of **CzT**. In hexane, the

Φ_F of **CzT** increases slightly from 4 to 7.4%, whereas a more evident increment of Φ_F from 14.3 to 45.6% in oxygen-free toluene was observed, indicating that an efficient up-conversion of **CzT** triplet excitons did occur. Fluorescence decay transients of **PhCzTAZ** in both hexane and toluene before and after N_2 treatment showed no delayed component In addition, only limited enhancements in Φ_F were observed, 3.3%→3.9% in hexane and from 4.4%→5.5% in toluene. This result is consistent with our speculation that the carbazole–triazine molecule **PhCzTAZ** with a different structural configuration will not exhibit TADF.

Temperature dependent fluorescence measurements of a 3 wt % **CzT**:DPEPO co-deposited film were conducted to ensure that the origin of observed delayed fluorescence of **CzT** is from TADF. In this case, room temperature fluorescence emission of **CzT** centred at 502 nm. In addition, the phosphorescence spectrum (77 K) of **CzT**:DPEPO co-deposited film showed a peak centred at 519 nm. The energy difference between S_1 and T_1 states, calculated from the onsets of the fluorescence and phosphorescence spectra is 90 meV. The PLQY of the **CzT**:DPEPO co deposited film was measured to be 39.7%. Temperature dependent fluorescence transients of a 3 wt% **CzT**:DPEPO film showed clearly delayed fluorescence at temperatures higher than 200 K. The intensity of the delayed fluorescence increased with increasing temperature. This behaviour is the signature feature of TADF as triplet excitons do not have enough energy for up-conversion at low temperatures.

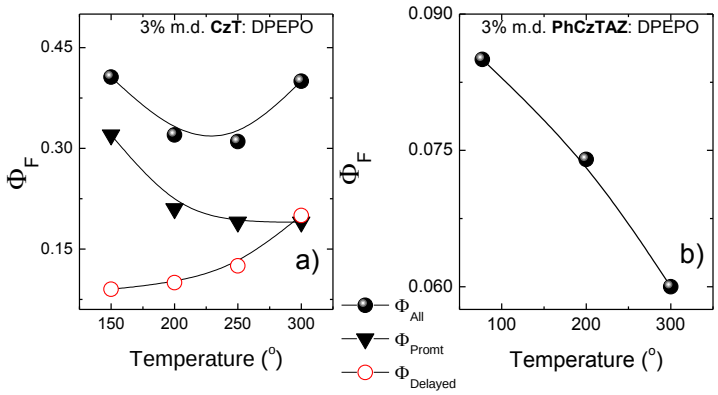

Fig. 5.5 a) Temperature dependence of fluorescence efficiency of 3 wt% **CzT**:DPEPO film: delayed fluorescence (◦), prompt fluorescence (▼) and total fluorescence (•). b) Temperature dependence of PL efficiency of 3 wt% **PhCzTAZ**:DPEPO film.

The efficiency of the delayed fluorescence (fig. 5.5) increases with increasing temperature from 150 K up to 300 K. Since the prompt fluorescence efficiency does not depend on the temperature in the temperature range of 200–300 K, the increase of overall fluorescence efficiency can be attributed to the assistance of TADF. When the temperature decreases below 200 K, the efficiencies of prompt and

total fluorescence increase probably due to the suppression of the non-radiative decay process In contrast, the fluorescence intensity (and Φ_F) of the **PhCzTAZ**:DPEPO co-deposited film decreases with increasing temperature due to the enhanced non-radiative relaxation rate. Fluorescence decay transients of the **PhCzTAZ:**DPEPO film revealed no delayed component. Additionally, Φ_F of a 3 wt% **PhCzTAZ**:DPEPO film was measured to be only 6%.

Electroluminescence properties. CzT was used in an OLED as a TADF emitter. The device was configured as: glass/ITO/a-NPD (30 nm)/TCTA (20 nm)/CzSi (10 nm)/3 wt% CzT:DPEPO (20 nm)/DPEPO (10 nm)/TPBi (30 nm)/LiF (0.8 nm)/Al (70 nm), where a-NPD, TCTA, CzSi and TPBI represent N,N0-diphenyl-N,N0-bis(1-naphthyl)-1,10- biphenyl-4,40-diamine,4,0,400-tris(N-carbazolyl) triphenylamine, 9-(4-tert-butylphenyl)-3,6-bis(triphenylsilyl)-9H-carbazole and 1,3,5- tris(N-phenylbenzimidazol-2-yl)benzene, respectively. The fabricated device gave blue-greenish electroluminescence centered at 520 nm. The EQE of the device was 6%, power efficiency of 9.7 lm W^{-1} and luminance of 393 cd m^{-2}.

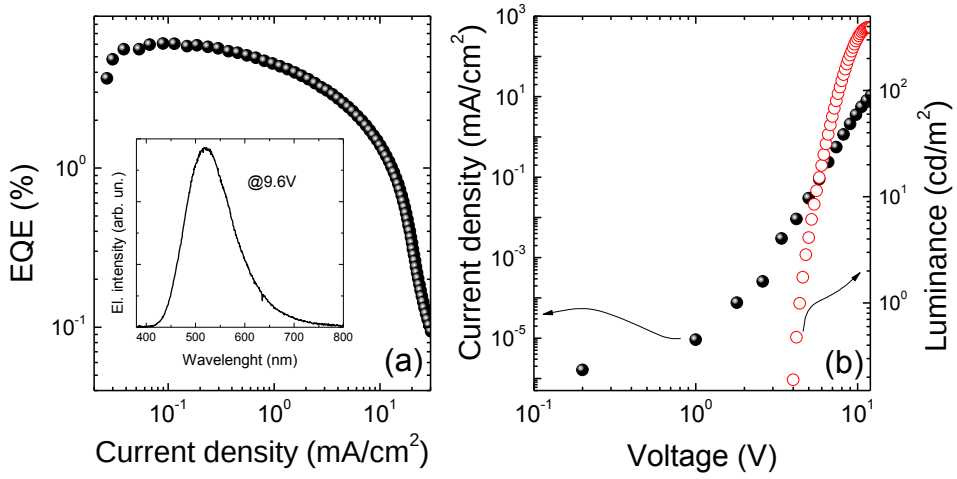

Fig. 5.6 (a) External quantum efficiency as a function of current density Inset: EL spectrum operated at 9.6 V (black line) of the device incorporating **CzT**. (b) Current density–voltage–luminance (J–V–L) characteristics of the device incorporating **CzT**.

The obtained 6% EQE of OLED with a **CzT**-doped emissive layer is about 3 times higher than the theoretical maximum value of 2% (with the assumption of out-coupling efficiency of 20%) when a conventional fluorescent emitter with PLQY of 39.7% was used. However, the maximum EQE value for OLED made from **CzT** as TADF emitter is 6.3% [46] and agrees well with the experimentally obtained value of 6%.

In conclusion, due to the reduced energy difference between the S_1 state and the T_1 state **CzT** possesses promising TADF properties with efficient triplet up-conversion. On the other hand, **PhCzTAZ**, consisting of carbazole and triazine components configured with a twisted conformation shows no evident TADF properties. Our observations clearly demonstrate that the TADF properties of carbazole–triazine materials are strongly affected by the structural configuration of electron-donating and -accepting components.

References

[1] http://www.oled-info.com/ubi-research-sees-25-billion-oled-emitter-material-market-2020

[2] http://www.oled-info.com/displaysearch-says-77000-oled-t(Vs)-were-sold-2014-generating-280-million-revenue

[3] http://www.oled-info.com/konica-minolta-developed-worlds-most-efficient-oled-panel-131-lmw

[4] http://www.oled-info.com/lg-chem-installs-worlds-biggest-building-oled-installation-1100-panels-snus-library

[5] J.-Y. Hu *et.al.*, "Bisanthracene-Based Donor-Acceptor-type Light-Emitting Dopants: Highly Efficient Deep-Blue Emission in Organic Light-Emitting Devices," *Adv. Funct. Mater.*, vol. 24, no. 14, p. 2064, 2014.

[6] H. Uoyama *et.al.*, "Highly efficient organic light-emitting diodes from delayed fluorescence," *Nature*, vol. 492, no. 7428, p. 234, 2012.

[7] C. W. Tang and S. A. VanSlyke, "Organic electroluminescent diodes," *Appl. Phys. Lett.*, vol. 51, no. 12, p. 913, 1987.

[8] C. Adachi *et.al.*, "Nearly 100% internal phosphorescence efficiency in an organic light-emitting device," *J. Appl. Phys.*, vol. 90, no. 10, p. 5048, 2001.

[9] Z. H. Kafafi, Ed., *Organic electroluminescence*. Boca Raton, FL: CRC Press, Taylor & Francis, 2005.

[10] C.-H. Chen *et.al.*, "Highly efficient orange and deep-red organic light emitting diodes with long operational lifetimes using carbazole–quinoline based bipolar host materials," *J. Mater. Chem. C*, vol. 2, no. 30, p. 6183, 2014.

[11] W. S. Jeon *et.al.*, "Ideal host and guest system in phosphorescent OLEDs," *Org. Electron.*, vol. 10, no. 2, pp. 240, 2009.

[12] D. Tanaka *et.al.*, "Ultra High Efficiency Green Organic Light-Emitting Devices," *Jpn. J. Appl. Phys.*, vol. 46, no. 1, pp. L10, 2007.

[13] J.-H. Jou *et.al.*, "Approaches for fabricating high efficiency organic light emitting diodes," *J Mater Chem C*, vol. 3, no. 13, p. 2974, 2015.

[14] K.-H. Kim *et.al.*, "Phosphorescent dye-based supramolecules for high-efficiency organic light-emitting diodes," *Nat. Commun.*, vol. 5, p. 4769, 2014.

[15] M. Kim *et.al.*, "Stable Blue Thermally Activated Delayed Fluorescent Organic Light-Emitting Diodes with Three Times Longer Lifetime than Phosphorescent Organic Light-Emitting Diodes," *Adv. Mater.*, vol 27, no. 15, p. 2515, 2015.

[16] A. Endo *et.al.*, "Thermally Activated Delayed Fluorescence from Sn4+-Porphyrin Complexes and Their Application to Organic Light Emitting Diodes - A Novel Mechanism for Electroluminescence," *Adv. Mater.*, vol. 21, no. 47, p. 4802, 2009.

[17] Y. Tao *et.al.* "Thermally Activated Delayed Fluorescence Materials Towards the Breakthrough of Organoelectronics," *Adv. Mater.*, vol. 26, no. 47, p. 7931, 2014.

[18] Q. Zhang *et.al.*, "Design of Efficient Thermally Activated Delayed Fluorescence Materials for Pure Blue Organic Light Emitting Diodes," *J. Am. Chem. Soc.*, vol. 134, no. 36, p. 14706, 2012.

[19] G. Méhes *et.al.*, "Enhanced Electroluminescence Efficiency in a Spiro-Acridine Derivative through Thermally Activated Delayed Fluorescence," *Angew. Chem. Int. Ed.*, vol. 51, no. 45, p. 11311, 2012.

[20] Q. Zhang *et.al.*, "Nearly 100% Internal Quantum Efficiency in Undoped Electroluminescent Devices Employing Pure Organic Emitters," *Adv. Mater.*, vol. 27, no. 12, p. 2096, 2015.
[21] D. Y. Kondakov, "Triplet-triplet annihilation in highly efficient fluorescent organic light-emitting diodes: current state and future outlook," *Philos. Trans. R. Soc. Math. Phys. Eng. Sci.*, vol. 373, no. 2044, p. 20140321, 2015.
[22] J. Huang *et.al.*, "The development of anthracene derivatives for organic light-emitting diodes," *J. Mater. Chem.*, vol. 22, no. 22, p. 10977, 2012.
[23] M. Pope, C. E. Swenberg, and M. Pope, *Electronic processes in organic crystals and polymers*, 2nd ed. New York: Oxford University Press, 1999.
[24] B. Valeur, *Molecular fluorescence: principles and applications*. Weinheim ; New York: Wiley-VCH, 2002.
[25] I. B. Berlman, *Handbook of fluorescence spectra of aromatic molecules*, 2d ed. New York: Academic Press, 1971.
[26] N. Nijegorodov *et.al.*, "The influence of planarity, rigidity and internal heavy atom upon fluorescence parameters and the intersystem crossing rate constant in molecules with the biphenyl basis," *Spectrochim. Acta. A. Mol. Biomol. Spectrosc.*, vol. 64, no. 1, p. 1 2006.
[27] N. Nijegorodov *et.al.*, "Photonics and photochemical stability of aromatic molecules, family related in π-structure but different in planarity, rigidity and molecule symmetry," *J. Photochem. Photobiol. Chem.*, vol. 196, no. 2–3, p. 219, 2008.
[28] K. N. Solov'ev and E. A. Borisevich, "Intramolecular heavy-atom effect in the photophysics of organic molecules," *Phys.-Uspekhi*, vol. 48, no. 3, p. 231, 2005.
[29] H. D. Becker, "Unimolecular photochemistry of anthracenes," *Chem. Rev.*, vol. 93, no. 1, p. 145, 1993.
[30] C. Adachi *et.al.*, "Blue light-emitting organic electroluminescent devices," *Appl. Phys. Lett.*, vol. 56, no. 9, p. 799, 1990.
[31] S.-K. Kim *et.al.*, "Exceedingly efficient deep-blue electroluminescence from new anthracenes obtained using rational molecular design," *J. Mater. Chem.*, vol. 18, no. 28, p. 3376, 2008.
[32] C.-L. Wu *et.al.*, "High efficiency non-dopant blue organic light-emitting diodes based on anthracene-based fluorophores with molecular design of charge transport and red-shifted emission proof," *Mater. Chem. C*, vol. 2, no. 35, p. 7188, 2014.
[33] S. C. Tse *et.al.*, "The role of charge-transfer integral in determining and engineering the carrier mobilities of 9,10-di(2-naphthyl)anthracene compounds," *Chem. Phys. Lett.*, vol. 422, no. 4–6, p. 354, 2006.
[34] B. Balaganesan *et.al.*, "Synthesis of t-butylated diphenylanthracene derivatives as blue host materials for OLED applications," *Tetrahedron Lett.*, vol. 44, no. 30, p. 5747, 2003.
[35] M.-H. Ho *et.al.*, "Highly efficient deep blue organic electroluminescent device based on 1-methyl-9,10-di(1 naphthyl)anthracene," *Appl. Phys. Lett.*, vol. 89, no. 25, p. 252903, 2006.
[36] M.-H. Ho *et.al.*," *Isr. J. Chem.*, vol. 52, no. 6, p. 484, 2012.
[37] S. W. Culligan *et.al.*, "Effect of Hole Mobility Through Emissive Layer on Temporal Stability of Blue Organic Light-Emitting Diodes," *Adv. Funct. Mater.*, vol. 16, no. 11, p. 1481, 2006.

[38] Y.-J. Pu *et.al.*, "Arylamino-9,10-diphenylanthracenes for organic light emitting devices," *Org. Electron.*, vol. 11, no. 3, p. 479, 2010.
[39] Y. Sun *et.al.*, "A Pyridine-Containing Anthracene Derivative with High Electron and Hole Mobilities for Highly Efficient and Stable Fluorescent Organic Light-Emitting Diodes," *Adv. Funct. Mater.*, vol. 21, no. 10, p. 1881, 2011.
[40] Z.-Q. Wang, C *et.al.*, Ji, "High-color-purity and high-efficiency non-doped deep-blue electroluminescent devices based on novel anthracene derivatives," *New J. Chem.*, vol. 36, no. 3, p. 662, 2012.
[41] J.-K. Bin and J.-I. Hong, "Efficient blue organic light-emitting diode using anthracene-derived emitters based on polycyclic aromatic hydrocarbons," *Org. Electron.*, vol. 12, no. 5, p. 802, 2011.
[42] K.-R. Wee *et.al.*, "Asymmetric anthracene-based blue host materials: synthesis and electroluminescence properties of 9-(2-naphthyl)-10-arylanthracenes," *J. Mater. Chem.*, vol. 21, no. 4, p. 1115, 2011.
[43] S. J. Strickler and R. A. Berg, "Relationship between Absorption Intensity and Fluorescence Lifetime of Molecules," *J. Chem. Phys.*, vol. 37, no. 4, p. 814, 1962.
[44] C.-J. Chiang *et.al.*, "Ultrahigh Efficiency Fluorescent Single and Bi-Layer Organic Light Emitting Diodes: The Key Role of Triplet Fusion," *Adv. Funct. Mater.*, vol. 23, no. 6, p. 739, 2013.
[45] H. Uoyama *et.al.*, "Highly efficient organic light-emitting diodes from delayed fluorescence," *Nature*, vol. 492, no. 7428, p. 234, 2012.
[46] H. Tanaka *et.al.*, "Efficient green thermally activated delayed fluorescence (TADF) from a phenoxazine–triphenyltriazine (PXZ–TRZ) derivative," *Chem. Commun.*, vol. 48, no. 93, p. 11392, 2012.

List of publications related to the thesis:

Papers:

S1. T. Serevičius, P. Adomėnas, O. Adomėnienė, R. Rimkus, V. Jankauskas, A. Gruodis, K. Kazlauskas, S. Juršėnas, Photophysical properties of 2-phenylanthracene and its conformationally-stabilized derivatives, *Dyes and Pigments*, 98, 304, (2013).

S2. T. Serevičius, P. Adomėnas, O. Adomėnienė, K. Karpavičius, J. Bucevičius, R. Komskis, V. Jankauskas, K. Kazlauskas, S. Juršėnas, Non-symmetric 2-phenylanthracene derivatives with improved charge transport properties, *Dyes Pigments*, 122, 147, (2015).

S3. T. Serevičius, R. Komskis, P. Adomėnas, O. Adomėnienė, V. Jankauskas, A. Gruodis, K. Kazlauskas, and S. Juršėnas, Non-symmetric 9,10-diphenylanthracene-based deep-blue emitters with enhanced charge transport properties, *Phys Chem Chem Phys*, 16, 7089, (2014).

S4. T. Serevičius, T. Nakagawa, M.-Ch. Kuo, Sh.-H. Cheng, K.-T. Wong, Ch.-H. Chang, R. C. Kwong, S. Xia, Ch. Adachi, Enhanced electroluminescence based on thermally activated delayed fluorescence from a carbazole–triazine derivative, *Phys Chem Chem Phys*, 15, 15850, (2013). *This article was chosen as a back-cover of PCCP journal, volume 15 (2013).*

Presentations at the conferences (underlined T. S. – presented personally):

K1 R. Komskis, P. Adomėnas, O. Adomėnienė, R. Rimkus, T. Serevičius, V. Jankauskas, A. Gruodis, K. Kazlauskas, S. Juršėnas, Nesimetriniai antraceno junginiai optoelektroniniams taikymams, Lietuvos nacionalinė fizikos konferencija, Vilnius, 2013.06.10-12.

K2 T. Serevičius, R. Komskis, P. Adomėnas, O. Adomėnienė, R. Rimkus, V. Jankauskas, A. Gruodis, K. Kazlauskas, A. Miasojedovas, S. Juršėnas, V. Jankus, A. Monkman,

2, 9, 10 substituted anthracene derivatives as blue fluorescent emitters, Optical Probes 2013, Durham, United Kingdom, 2013.07.14-19.

K3 T. Serevičius, R. Komskis, P. Adomėnas, O. Adomėnienė, V. Jankauskas, A. Gruodis, K. Kazlauskas, S. Juršėnas, Control of fluorescence and charge transfer properties of anthracene derivatives, Electronic processes in Organic Materials, Barga, Italy, 2014.05.04-09.

K4 T. Serevičius, R. Komskis, P. Adomėnas, O. Adomėnienė, V. Jankauskas, A. Gruodis, K. Kazlauskas, S. Juršėnas, Nonsymmetric 2,9,10-diphenylanthracene-based deep-blue emitters with enhanced charge transport properties, XVth International Krutyn Summer School 2014, Krutyn, Poland, 2014.06.08-14.

K5 T. Serevičius, P. Adomėnas, O. Adomėnienė, R. Rimkus, V. Jankauskas, A. Gruodis, R. Komskis, K. Kazlauskas, S. Juršėnas, Non-symmetric anthracene derivatives with advanced film forming, emission and charge transport properties, XXIII International Materials Research Congress, Cancun, Mexico, 2014.08.17-21.

K6. T. Serevičius, R. Komskis, R. Rimkus, S. Tumkevičius, P. Adomėnas, A. Gruodis, V. Jankauskas, K. Kazlauskas, S. Juršėnas, Epoxydinaphtocarbazole derivatives for optoelectronics, 13th European Conference on Molecular Electronics, Strasbourg, France, 2015.09.01-05.

Patents:

P1 2014.03.25 **Patent of Lithuanian Republic** (Nr. 6012). S. Juršėnas, S. Tumkevičius, K. Kazlauskas, V. Jankauskas, T. Serevičius, P. Adomėnas, R. Rimkus, "Nauji 1,5-dipakeisti 11-oksa-3-aza-3H-3-alkil- (arba aril-) dibenzo[a,m]indeno[2,1,7,6-ghij]pleiadenų junginiai, jų sintezė ir taikymas optoelektronikoje“.

P2 2015.01.26 **Patent of Lithuanian Republic** (Nr. 6153). S. Juršėnas, K. Kazlauskas, V. Jankauskas, T. Serevičius, R. Komskis, O. Adomėnienė, P. Adomėnas, „Nauji 2,2’,10,10’-pakeisti 9,9’-biantracenai, jų sintezė ir taikymas optoelektronikoje“.

Author's contribution

The author of this thesis made all the experiments of optical characterisation of all materials and made the analysis of data, combined the obtained results with those additional (DFT calculations, DSC measurements, photoelectrical measurements) provided by co-authors from other research groups and provided critical analysis and suggestions of further improvements. The author also prepared manuscripts of papers, participated in preparation of conference presentations and made presentations in the majority of conferences itself. Anthracene compounds were synthesized by dr. P. Adomėnas group from Liquid crystal laboratory (Institute of Applied Research, Vilnius University). A part of results were obtained in collaboration with other laboratories: DFT calculations were performed by ass. prof. Alytis Gruodis (Department of general physics and spectroscopy, Vilnius University) and Gediminas Kreiza (Institute of Applied Research, Vilnius University); charge mobility and ionization potential measurements were performed by ass. prof. Vygintas Jankauskas (Department of Solid State Electronics, Vilnius University), DSC measurements were performed by Sandra Mačiulytė (Department of Polymer Chemistry, Vilnius University). The research of thermally activated delayed fluorescence (measurements of fluorescence properties, OLED fabrication and electroluminescence research) was performed during the stay in Center of Organic Electronics and Photonics Research, Kyushu University, under the supervision of prof. Chihaya Adachi and in collaboration with dr. Tetsuya Nakagawa and Munetomo Inoue.

Information about the author:

1. **First name** Tomas
2. **Second name** Serevičius
3. **Birth date** 1986.03.27
4. **Phone and email** +37052366028, tomas.serevicius@ff.stud.vu.lt

5. **Education**

Place	Year	Degree/Program
Vilniaus University	2015	Doctoral studies
Vilniaus University	2011	Master/Material Science and Semiconductor Physics
Vilniaus University	2009	Bachelor/Physics of Modern Technologies
Viršuliškės Secondary school	2005	Secondary education

6. **Scientific work experience**

Year	Institucija	Pareigos
2014	Centre of Organic Photonics and Electronics Research/Kyushu University	Visiting researcher
2013 –	Vilnius University/ Institute of Applied Research	Junior researcher
2013	Centre of Organic Photonics and Electronics Research/Kyushu University	Visiting researcher
2010	Linkoping University	Visiting student
2009 – 2013	Vilnius University/ Institute of Applied Research	Engineer
2007 – 2009	Vilnius University/ Institute of Applied Research	Technician